THE ASTROPHYSICAL JOURNAL, 449:L65–L68, 1995 August 10

GRAVITATIONAL INFALL IN THE DENSE CORES L1527 AND L483

P. C. MYERS,[1] R. BACHILLER,[2] P. CASELLI,[1] G. A. FULLER,[3] D. MARDONES,[1] M. TAFALLA,[1] AND D. J. WILNER[1]
Received 1995 April 24; accepted 1995 May 26

ABSTRACT

Lines of N_2H^+, C_3H_2, and H_2CO show kinematic evidence of gravitational infall in L1527, and probably also in L483. Three trends appear to indicate infall, rather than outflow or rotation: (*a*) at each protostar position, line peak and centroid velocities get bluer by 0.1–0.3 km s^{-1} with increasing line optical depth; (*b*) in maps of C_3H_2 and H_2CO lines, peak and centroid velocities get bluer by a similar amount as positions approach each protostar; and (*c*) C_3H_2 line widths in L1527 increase as positions approach the protostar. Also, in both sources H_2CO lines show the infall "signature" of spatially concentrated double-peaked profiles, with their blue peaks brighter than their red peaks, as seen previously in B335. Many asymmetric profiles have a single blueshifted peak with a red shoulder, or two peaks with blue/red intensity ratio greater than 3. These are hard to fit with spherical infall models, owing perhaps to the effects of the bipolar outflow. In each source, H_2CO line wings show clear evidence of collimated outflow.

Subject headings: ISM: molecules — line: profiles — stars: formation

1. INTRODUCTION

All models of star formation are based on inward gravitational motions, but such motions have little observational basis. The best targets for infall searches are the youngest far-infrared sources within a few hundred parsecs of the Sun, around which gas motions can be spatially resolved. These sources have central locations in maps of dense gas, very red spectral energy distributions, and highly collimated molecular outflows. The spectral redness is indicated by the steepness of the mid-infrared spectrum (Lada 1991), by the ratio of submillimeter to infrared flux (André, Ward-Thompson, & Barsony 1993, hereafter AWB) or by the equivalent-blackbody ("bolometric") temperature T_{bol} (Myers & Ladd 1993).

Three of the best infall candidates are the low-luminosity (1–10 $L_\odot$) sources with "class 0" (AWB) spectra, centrally located in NH_3 maps in B335, L1527, and L483 (Benson & Myers 1989; Fuller & Myers 1993), having T_{bol} = 34, 59, and 49 K, respectively (Ladd et al. 1991; Chen et al. 1995), and having evidence for collimated outflows (Hirano et al. 1992; Parker, Padman, & Scott 1991). The best case for gravitational infall among such nearby regions is in B335 (Zhou et al. 1993; Chandler & Sargent 1993). There, H_2CO and CS line profiles have a brighter blue peak and a fainter red peak, and spatial concentration of this shape toward the infrared source. These properties are consistent with spherically symmetric "inside-out" collapse (Shu 1977), according to detailed models by Zhou et al. (1993).

This paper summarizes our high-resolution observations of L1527 and L483, in 3 mm lines of C_3H_2 and N_2H^+, and in 2 mm and 1 mm lines of H_2CO. In § 2.1 we show two-peak asymmetry in the C_3H_2 and H_2CO lines, similar to that seen in B335, and we identify a more general and more prevalent blueshifted asymmetry in the line shapes. In § 2.2 we present three systematic properties of the line profiles, and in § 3 we interpret these trends to indicate infall, as opposed to outflow or rotation.

[1] Harvard-Smithsonian Center for Astrophysics, 60 Garden Street, Cambridge, MA 02138; myers, caselli, mardones, tafalla, wilner@cfa.harvard.edu.
[2] Centro Astronómico de Yebes (IGN), Apartado 148, E-19080, Guadalajara, Spain; bachiller@cay.es.
[3] National Radio Astronomy Observatory, Edgemont Road, Charlottesville, VA 22903; gfuller@nrao.edu. NRAO is operated by Associated Universities, Inc., under cooperative agreement with the National Science Foundation.

2. OBSERVATIONS AND RESULTS

We observed the lines in Table 1 in 1993–1994 and 1994–1995 winter at the 37 m NEROC Haystack telescope[4] and in 1994 September at the 30 m IRAM telescope. We took spectra over 1′–3′ in each source, to define how the profiles vary with position, especially along and across the outflow direction. The Haystack observations were first reported by Mardones et al. (1994).

2.1. *Line Profiles*

The line profiles toward each candidate protostar have, to varying degrees, wings at high velocities and multiple peaks and asymmetry at low velocities. Figure 1 shows lines of C_3H_2 observed at Haystack and of N_2H^+ and H_2CO observed at IRAM, toward IRAS 04368+2557 in L1527 and toward IRAS 18148−0440 in L483.

Both H_2CO lines have wings extending over several kilometers per second, more prominently in L483 than in L1527. In our maps, these wings shift to the blue in the west and to the red in the east for each source. These shifts have the same sign, and similar space direction, as do the ^{12}CO outflow wings, mapped in L1527 (MacLeod et al. 1994) and in L483 (Fuller et al. 1995). Thus the H_2CO line wings indicate outflow motions of gas denser than 10^5 cm^{-3} (Mangum & Wootten 1993). In contrast, the C_3H_2 and N_2H^+ lines show no such wings in either source.

A two-peak asymmetry, with a brighter blue peak and a fainter red peak, is seen in Figure 1, in both H_2CO lines and in the C_3H_2 line in L1527 and the 2 mm H_2CO line in L483. The peaks are separated by a self-absorption dip at velocities where the N_2H^+ line has peak intensity. This two-peak shape was seen in H_2CO lines in B335 and L1527 (Zhou et al. 1993, 1994b), and is the best-known signature of infall (e.g., Leung & Brown 1977). The H_2CO spectra of L1527 and L483 in Figure

[4] Radio astronomy observations at the Haystack Observatory of the Northeast Radio Observatory Corporation are supported by a grant from the National Science Foundation.

TABLE 1

OBSERVATIONAL PARAMETERS

Telescope	f (GHz)	Molecule	Transition	η_b	$\Delta\theta_b$
Haystack 37 m.....	85.3	C_3H_2	2_{12}–1_{01}	0.2	24″
	93.2	N_2H^+	1–0	0.2	22
IRAM 30 m	85.3	C_3H_2	2_{12}–1_{01}	0.71	29
	93.2	N_2H^+	1–0	0.70	27
	96.4	$C^{34}S$	2–1	0.68	26
	140.8	H_2CO	2_{12}–1_{11}	0.62	17
	225.7	H_2CO	3_{12}–2_{11}	0.53	11

NOTE.—Line frequencies are given in Vrtilek, Gottlieb, & Thaddeus 1987 for C_3H_2, and in Lovas 1986 for all others, except for N_2H^+. The N_2H^+ $JF_1F = 101 \rightarrow 012$ quadrupole hyperfine component has frequency 93176.265 ± 0.007 MHz (Caselli & Myers 1995). The main-beam efficiency η_b is the ratio of atmosphere-corrected antenna temperature (T_A^*) to main-beam brightness temperature (T_{mb}). The FWHM beamwidth $\Delta\theta_b$ and η_b are from Barvainis et al. 1993 and Baars et al. 1993. The Haystack system temperature was typically 250 K, and the spectral resolution 10 kHz. The IRAM system temperature and spectral resolution were typically 300 K and 10 kHz at 3 mm, 400 K and 20 kHz at 2 mm, and 800 K and 40 kHz at 1 mm. The observations used in-band frequency switching at Haystack, and position switching at IRAM, with reference position 4′ east. The Haystack and IRAM velocity scales differ by 0.00 ± 0.02 km s^{-1} according to our observations of L483 in the 2_{12}–1_{01} line of C_3H_2. The 1 mm and 2 mm H_2CO line velocities in L483 each have night-to-night differences less than 0.01 ± 0.03 km s^{-1}.

1 indicate outflow and infall in the same spectra, more clearly than in B335.

Nearly all of the lines in Figure 1 have blueshifted asymmetry, with or without a self-absorption dip. The L483 lines of 1 mm H_2CO, of C_3H_2, and of N_2H^+ have single peaks which are skewed to the blue, and/or they have red "shoulders." Our map data also show that lines with asymmetry have more single peaks than double and have more red shoulders than blue. In some cases the red-shoulder and double-peak line shapes are nearly indistinguishable. Red-shoulder lines in L1527 have also been reported in the $J = 2$–1 transition of $C^{18}O$ (Zhou et al. 1994b).

Figure 2 shows profiles of the 2 mm H_2CO line in L1527 along north-south and east-west cuts through the *IRAS* source. The outflow wings coincide approximately with the small-scale CO $J = 3$–2 outflow features seen in the blue to the west and in the red to the northeast by MacLeod et al. (1994). Also, the spectra have either two-peak or red-shoulder asymmetry extending over ~0.04 pc in seven of 13 positions, including the center; in two positions along the outflow; and in four positions across the outflow. Most profiles with two peaks have a ratio of blue to red intensity greater than 3, much greater than the ratios 1–2 seen in the 1 mm H_2CO line in L1527 or in the 2 mm line in B335 (Zhou et al. 1993).

2.2. *Line Velocities, Widths, and Optical Depths*

For both L1527 and L483, Figure 1 shows that the velocity of peak emission tends to decrease, from the lines of N_2H^+ to C_3H_2 to 1 mm H_2CO to 2 mm H_2CO, by a total of 0.2–0.3 km s^{-1}. For greater precision we computed the centroid velocity and its 1 σ error from the first moment of each spectrum over a 2 FWHM velocity range. We then formed the differences in centroid velocity from N_2H^+ to each of the other three lines in L1527 and in L483. Of these six differences, all but one (1 mm H_2CO in L483) follow the foregoing progression in the velocities of peak emission, from N_2H^+ to 2 mm H_2CO, and they exceed their 1 σ error. The largest differences are from N_2H^+ to 2 mm H_2CO, 0.25 ± 0.06 km s^{-1} in L1527 and 0.33 ± 0.02 km s^{-1} in L483.

The outflow wings on the 2 mm H_2CO spectra in L1527 do not significantly affect these centroid velocities because over the window of integration the wings are weaker than the peak, and are approximately symmetrical with respect to the centroid. Similarly, the trends are not due to an error in the rest frequency of N_2H^+, since the optically thin line of $C^{34}S$, also observed with the 30 m telescope, shows the same velocity as the N_2H^+ line, within its uncertainty, in L1527, and a marginally larger velocity, by 0.04 ± 0.03 km s^{-1}, in L483.

The centroid velocities get bluer in a second way, as positions approach each protostar. This tendency is evident in Figure 2 for L1527 in the 2 mm H_2CO line, and it is shown quantitatively in Figure 3 for the N_2H^+, C_3H_2, and 2 mm H_2CO lines. There the centroid velocity varies with beam position along four tracks passing through the protostar. As positions approach the protostar, the velocity of the 2 mm H_2CO line gets distinctly bluer, or decreases, by 0.1–0.4 km s^{-1}. The velocity of the C_3H_2 line decreases less, by 0.0–0.2 km s^{-1}. Of the eight tracks in the H_2CO and C_3H_2 lines, six show a significant velocity decrease toward the protostar. The N_2H^+ line shows no significant trend.

The centroid velocity trends are not symmetrical along each track: the C_3H_2 centroid has negligible decrease, 0.02 km s^{-1}, as positions approach the protostar from the northwest (*diamonds on left*), but a larger and significant decrease, 0.19 km s^{-1}, approaching from the southeast (*diamonds on right*). Similarly, the gradient in the northeast slightly exceeds that in

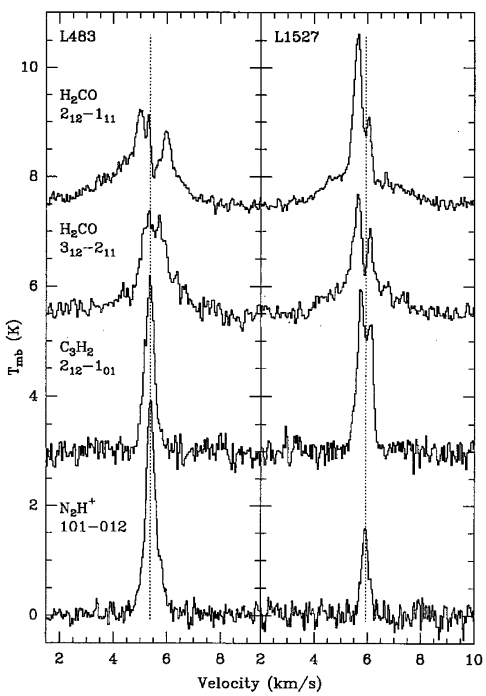

FIG. 1.—Spectra observed toward the candidate protostars IRAS 04368+2557 (1950 R.A., decl. = 04^{h}36^{m}49^s.3, 25°57′16″) in L1527, and IRAS 18148−0440 (18^{h}14^{m}50^s.6, −04°40′49″) in L483. Spectra have resolution 0.05 km s^{-1}. Lines of H_2CO and N_2H^+ were uniformly averaged over the central 3 × 3 grid with 10″ spacing. Thus all spectra have FWHM resolution ~30″, or 0.02 pc in L1527 assuming 140 pc distance (Elias 1978) and 0.03 pc in L483, assuming 200 pc (Parker et al. 1991). *Dotted line*: Centroid velocity of the N_2H^+ transition. Velocities of peak emission tend to shift to the blue, from lines of N_2H^+ to C_3H_2 to H_2CO.

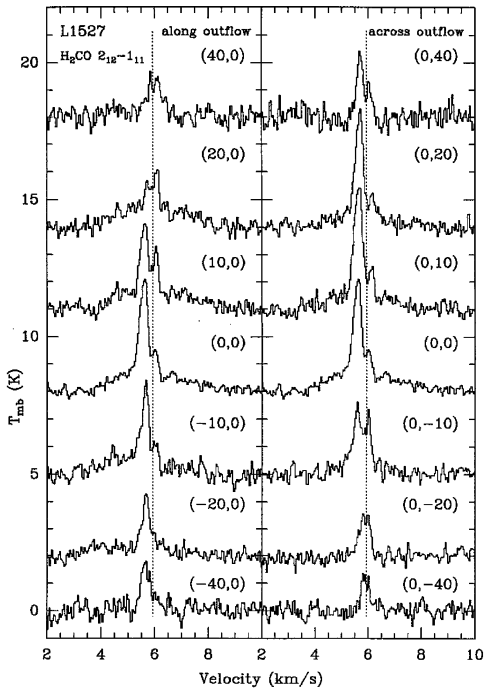

FIG. 2.—Spectra of the 2 mm $J_{K-K+} = 2_{12}$–1_{11} line of H_2CO along north-south and east-west tracks in L1527, centered on IRAS 04368+2557. *Dotted line*: As in Fig. 1. Velocities of peak emission shift to the blue as in Fig. 1, as map positions approach the *IRAS* source.

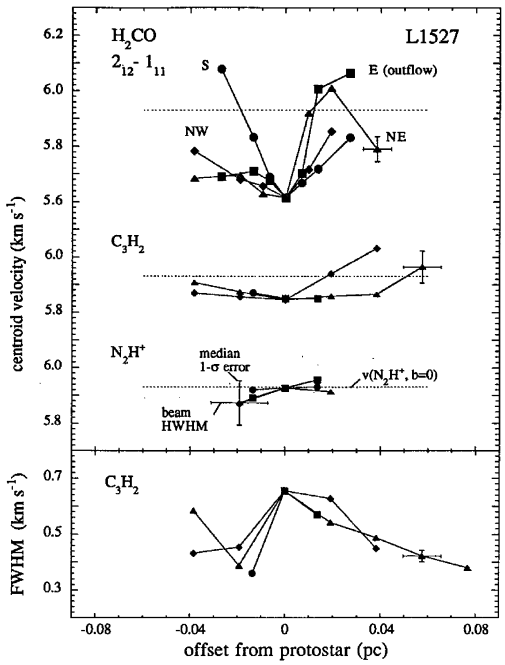

FIG. 3.—Spatial variation of line centroid and width in L1527 vs. offset of the beam from the protostar, along tracks passing through the protostar. Offsets increase from south to north (*circles*), from west to east (*squares*), from southwest to northeast (*triangles*), and from northwest to southeast (*diamonds*). *Upper panel*: Centroid velocities with 1 σ error $\leq$ 0.13 km s^{-1}, for lines with decreasing optical depth, from H_2CO to N_2H^+. Error bars indicate beam FWHM and median 1 σ centroid error. *Dotted line*: As in Fig. 1. Centroid velocities get progressively bluer as positions approach the protostar. *Lower panel*: Variation of C_3H_2 FWHM, based on Gaussian fits. These line widths broaden as positions approach the protostar.

the southwest for both the C_3H_2 and 2 mm H_2CO lines. However, the 2 mm H_2CO velocity trend along the outflow direction (east-west) is indistinguishable from the trends in the nonoutflow directions. As a test, we subtracted Gaussian fits to the 2 mm H_2CO line wings, computed centroid velocities of the residual spectra, and found no significant change from the trend in Figure 3.

The L483 line velocities (not shown) decrease with position as do those in L1527. The peak and centroid velocities of N_2H^+ and C_3H_2 each decrease by 0.0–0.3 km s^{-1} as positions approach the protostar over a distance of 0.04 pc. The 2 mm H_2CO emission in L483 shows a similar trend in its peak velocities. However, the corresponding 2 mm H_2CO centroid velocities are more affected by the outflow, and have more complex variation with position.

Figure 3 shows a third property: the FWHM of the C_3H_2 line increases from 0.4 to 0.6 km s^{-1} as positions approach the protostar in L1527. A similar increase in C_3H_2 line width is seen in B335 (Mardones et al. 1995) but not in L483.

The systematic decrease in line velocity from N_2H^+ to H_2CO in Figure 1 appears to correlate with increasing line optical depth. The peak optical depth of the $JF_1F = 101 \rightarrow 012$ component of the N_2H^+ line in Figure 1 is estimated from fits to the seven-component hyperfine structure to be 0.7 in L1527 and 1.2 in L483. The modest self-absorption dips and shoulders in the C_3H_2 lines in L1527 and L483 suggest that the C_3H_2 lines are generally optically thicker than the N_2H^+ lines. The deeper dips in the 1 mm and 2 mm H_2CO profiles at many positions in both sources suggest that their peak optical depths are significantly greater than those of either N_2H^+ or C_3H_2. The models described in § 3.2 are consistent with this ranking, indicating peak optical depths in L1527 of ~3, 11, and 16 for the lines of C_3H_2, 1 mm H_2CO, and 2 mm H_2CO.

3. DISCUSSION

3.1. *Infall, Outflow, and Rotation*

The two systematic decreases in centroid velocity described above probably arise from systematic motions, most likely infall, outflow, rotation, or a combination. Among these choices, infall motions are most nearly consistent with simple models. For spherically symmetric models of gas with inward motions and centrally elevated excitation temperature, line centroids are skewed to the blue with increasing optical depth, as line profiles progress from single-peaked with symmetric shape, to single-peaked with peak skewed to the blue, to double-peaked with the blue peak brighter than the red peak (e.g., Zhou 1992; Walker, Narayanan, & Boss 1994). In such models the blue part of the line profile arises from the rear of the cloud, the red part from the front of the cloud, and the dip, if present, from low-excitation, low-velocity foreground gas.

The observed decrease in centroid velocity with position is not expected for outward radial motions, which give increases rather than decreases in centroid velocity toward the source. It is also not expected for other motions with symmetry about the protostar, including rotation (Adelson & Leung 1988), bipolar outflow (Cabrit & Bertout 1990), and shear: these yield velocity gradients of the same sign on both sides of the source, rather than of opposite sign as seen here. However, infall with some other motion, such as rotation, might account for the asymmetric tracks in Figure 3.

The increase in C_3H_2 line width as position approaches the protostar in L1527, shown in Figure 3, seems unlikely to arise

from outflow motions, since the C_3H_2 line shows no indication of outflow wings, unlike the H_2CO lines. It is not due to uniform rotation, since the corresponding velocity gradient of a few km s^{-1} pc^{-1} is not seen over the line maps. An increase in optical depth from 1 to 3 in a static cloud would broaden the line by a factor of 1.3, somewhat less than the observed 1.6. The observed broadening of 0.2 km s^{-1} over radius 0.03 pc corresponds to protostar mass 0.4 $M_\odot$ and inside-out collapse age 0.2 Myr (Shu 1977).

3.2. *Infall with and without Spherical Symmetry*

We have used two independent radiative transfer codes to model the observed line profiles in L1527. The larger code solves the radiative transfer and the molecular energy level populations self-consistently for a spherically symmetric cloud (Auer 1991; Dickel & Auer 1994). Efforts to fit the observed H_2CO lines in L1527 following the Zhou et al. (1993, 1994a) prescription for inside-out collapse are generally successful for lines with a ratio of blue to red peak intensities of 1–2, as shown in Figure 4 for the 1 mm line. In these cases the model input parameters are similar to those of Zhou et al. (1994a) in B335, and they yield similar infall motions, ~0.1 km s^{-1} over size scales ~0.02 pc. The smaller code more simply integrates the equation of radiative transfer for a specified run of density and excitation temperature, with trapping implicit, but allows for departures from front-back symmetry along the line of sight. Assuming front-back symmetry, this code also succeeds in reproducing observed C_3H_2 and H_2CO line profiles in L1527, for similar input parameters, provided that the ratio of blue to red peak intensities is again 1–2.

Two-peak lines with blue/red intensity ratio greater than 3, or single-peak lines with red shoulders, as in the 2 mm H_2CO lines in L1527 (Figures 2 and 4), appear difficult to fit with either code. The smaller code can fit such profiles only if the front and back distributions of density differ. One form of the needed change is a density decrease over a zone smaller than 0.01 pc in the front half of the core. Such a reduction could be associated with the bipolar outflow, and future infall models should include the effects of outflows.

In summary, the blueshift of the centroid velocity with increasing optical depth, in lines of C_3H_2 and H_2CO in L1527 and L483, appears more nearly consistent with gravitational infall than with outflow or rotation, and may prove useful for infall searches and comparison with models. The increase in C_3H_2 line width toward the protostar in L1527 also appears more consistent with infall than with outflow or rotation.

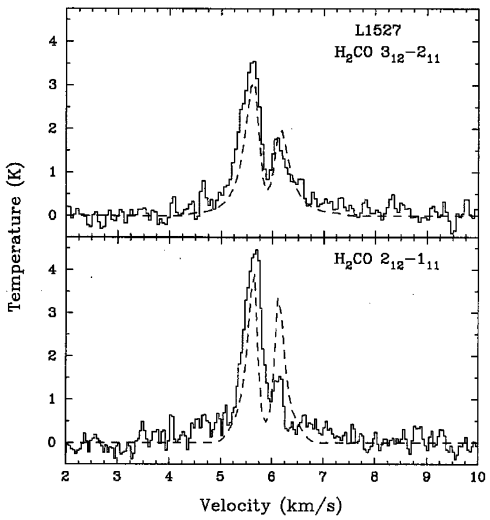

FIG. 4.—Spectra of H_2CO lines toward the protostar in L1527, as observed (*solid line*) and modeled (*dashed line*). The model velocity and density profiles are given by the Shu (1977) inside-out collapse solution, for sound speed 0.25 km s^{-1} and central mass 0.2 $M_\odot$. The kinetic temperature profile is assumed to be (30 K)$(r/100\ \mathrm{AU})^{-0.3}$, with a lower bound of 12 K. Local microturbulent broadening is assumed to have FWHM = 0.15 km s^{-1}. The H_2CO abundance is 2.0×10^{-9}. The spectra have been smoothed with the appropriate Gaussian beams of FWHM 12″ (0.0082 pc) and 17″ (0.012 pc). The model fits the spectrum much better when the ratio of blue to red peak intensity is less than 2 (*upper panel*) than when it is greater than 2 (*lower panel*).

L1527 has a better case for simple infall, while L483 is more complex and has a more prominent outflow. Even L1527 shows clear departures from spherical symmetry. More conclusive determination and study of infall motions will require more sources, having unbiased selection, multiple lines, and maps with finer resolution.

We thank the staff of Haystack Observatory and of the IRAM 30 m telescope, whose assistance made these observations possible. This work was supported by the NASA Origins of Solar Systems Program, grant NAGW-3401. R. B. acknowledges support from the Spanish DGICYT grant PB93-48. P. C., G. A. F., D. M., and D. J. W. acknowledge fellowship support from Smithsonian Astrophysical Observatory, National Radio Astronomy Observatory, Carnegie Institution of Washington, and the Harvard-Smithsonian Center for Astrophysics, respectively.

REFERENCES

Adelson, L. M., & Leung, C. M. 1988, MNRAS, 235, 349
André, P., Ward-Thompson, D., & Barsony, M. 1993, ApJ, 406, 122 (AWB)
Auer, L. H. 1991, in Stellar Atmospheres: Beyond Classical Models, ed. L. Crivellari, I. Hubeny, & D. G. Hunter (Dordrecht: Kluwer), 9
Baars, J., Greve, A., Hein, H., Morris, D., Penalver, J., & Thum, C. 1993, IRAM Rep. 298
Barvainis, R., Ball, J. A., Ingalls, R. P., & Salah, J. E. 1993, PASP, 105, 1334
Benson, P. J., & Myers, P. C. 1989, ApJS, 71, 89
Cabrit, S., & Bertout, C. 1990, ApJ, 348, 530
Caselli, P., & Myers, P. C. 1995, in preparation
Chandler, C. J., & Sargent, A. I. 1993, ApJ, 414, L29
Chen, H., Ladd, E. F., Myers, P. C., & Wood, D. O. 1995, ApJ, 445, 377
Dickel, H. R., & Auer, L. H. 1994, ApJ, 437, 222
Elias, J. H. 1978, ApJ, 224, 857
Fuller, G. A., Lada, E. A., Masson, C. R., & Myers, P. C. 1995, ApJ, in press
Fuller, G. A., & Myers, P. C. 1993, ApJ, 418, 273
Hirano, N., Kameya, O., Kasuga, T., & Umemoto, T. 1992, ApJ, 390, L85
Lada, C. J. 1991, in The Physics of Star Formation and Early Stellar Evolution, ed. C. J. Lada & N. D. Kylafis (Dordrecht: Kluwer), 329
Ladd, E. F., Adams, F. C., Casey S., Davidson, J. A., Fuller, G. A., Harper, D. A., Myers, P. C., & Padman, R. 1991, ApJ, 366, 203
Leung, C. M., & Brown, R. B. 1977, ApJ, 214, L73
Lovas, F. J. 1986, J. Chem. Phys. Ref. Data, 15, 251
MacLeod, J., Avery, L., Harris, A., & Tacconi, L. 1994, JCMT Newsletter, September/October, 46
Mangum, J. G., & Wootten, H. A. 1993, ApJS, 89, 123
Mardones, D. M., Caselli, P., Fuller, G. A., Myers, P. C., Tafalla, M., & Wilner, D. J. 1995, in preparation
Mardones, D. M., Myers, P. C., Caselli, P., & Fuller, G. A. 1994, in Clouds, Cores, and Low Mass Stars, ed. D. Clemens & R. Barvainis (San Francisco: ASP), 192
Myers, P. C., & Ladd, E. F. 1993, ApJ, 413, L47
Parker, N. D., Padman, R., & Scott, P. F. 1991, MNRAS, 252, 442
Shu, F. H. 1977, ApJ, 214, 488
Vrtilek, J. M., Gottlieb, C. A., & Thaddeus, P. 1987, ApJ, 314, 716
Walker, C. K., Narayanan, G., & Boss, A. P. 1994, ApJ, 431, 767
Zhou, S. 1992, ApJ, 394, 204
Zhou, S., Evans, N. J., Kompe, C., & Walmsley, C. M. 1993, ApJ, 404, 232
———. 1994a, ApJ, 421, 854
Zhou, S., Evans, N. J., Wang, Y., Peng, R., & Lo, K. Y. 1994b, ApJ, 433, 131